Pressure-induced structural phase transition in the IV–VI semiconductor SnS

2004 J. Phys.: Condens. Matter 16 3545

(http://iopscience.iop.org/0953-8984/16/21/004)

INSTITUTE OF PHYSICS PUBLISHING JOURNAL OF PHYSICS: CONDENSED MATTER

J. Phys.: Condens. Matter **16** (2004) 3545–3554 PII: S0953-8984(04)76002-6

Pressure-induced structural phase transition in the IV–VI semiconductor SnS

L Ehm[1,2,5], K Knorr[1], P Dera[2], A Krimmel[3], P Bouvier[4] and M Mezouar[4]

[1] Institut für Geowissenschaften, Mineralogie/Kristallographie, Christian-Albrechts-Universität zu Kiel, Olshausenstraße 40, 24098 Kiel, Germany
[2] Geophysical Laboratory, Carnegie Institution of Washington, 5251 Broad Branch Road NW, Washington, DC 20015, USA
[3] Experimentalphysik V, Elektronische Korrelationen und Magnetismus, Institut für Physik, Universität Augsburg, 86135 Augsburg, Germany
[4] ESRF, BP 220, Grenoble Cedex, France

E-mail: l.ehm@gl.ciw.edu

Received 6 February 2004
Published 14 May 2004
Online at stacks.iop.org/JPhysCM/16/3545
DOI: 10.1088/0953-8984/16/21/004

Abstract

The structural behaviour of SnS under high-pressure has been investigated by angular dispersive synchrotron powder diffraction up to 38.5 GPa. A structural phase transition from orthorhombic α-SnS to monoclinic γ-SnS was observed at 18.15 GPa. The fit of a Birch–Murnaghan equation-of-state gave the volume at zero pressure of $V_0 = 192.6(3)$ Å^3, the bulk modulus at zero pressure of $B_0 = 36.6(9)$ GPa and the pressure derivative of the bulk modulus $B' = 5.5(2)$ for α-SnS and $V_0 = 160(1)$ Å, $B_0 = 86.0(5)$ GPa and $B' = 4$ for γ-SnS. The improper ferro-elastic transition is of first-order and is accompanied by a large volume discontinuity of about 9.1%. The phase transition can be described in terms of a group/subgroup relationship. The doubling of the unit cell indicates a wavevector $(1/2, 0, 1/2)$ at the U-point in the Brillouin zone.

1. Introduction

Layered IV–VI semiconductors, e.g. GeS, GeSe, α-SnS, SnSe, have been attracting much scientific interest due to their potential applications in optoelectronic devices [1–4]. Tin sulfide, α-SnS, crystallizes in space group $Pnma$ in the GeS (B16) type structure with lattice parameters of $\mathbf{a} = 11.200(2)$ Å, $\mathbf{b} = 3.987(1)$ Å and $\mathbf{c} = 4.334(1)$ Å. Sn and S occupy the Wyckoff position 4c $(x, 1/4, z)$ with fractional coordinates $x = 0.1194(1), z = 0.1198(2)$ for tin and $x = 0.8508(3), z = 0.4793(8)$ for sulfur [5–7]. The structure consists of SnS double layers stacked onto each other along the **a**-axis (figure 1). Each atom is coordinated by three strongly (2.627–2.665 Å) and two weakly (3.290 Å) bound neighbours in the layer and one

[5] Author to whom any correspondence should be addressed.

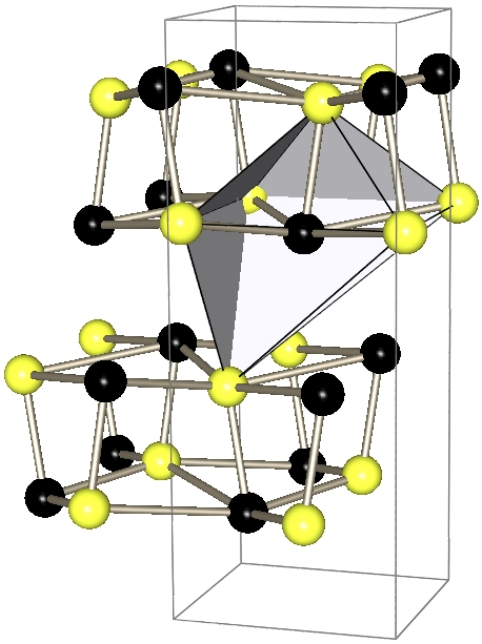

Figure 1. Crystal structure of α-SnS. The black spheres represent tin atoms and the light grey spheres are sulfur atoms. The coordination polyhedron of tin is plotted in light grey.

(This figure is in colour only in the electronic version)

(3.494 Å) in the adjacent layer. This results in a 3 + 3 coordination forming a highly distorted octahedron [7]. The rare mineral herzenbergite is the natural analogue to α-SnS and can be found in silver–tin ore deposits, e.g. the Maria Teresia Mine in Huari, Bolivia [8].

The electronic and optical properties of α-SnS and isostructural IV–VI semiconductors have been extensively studied experimentally by electron-energy-loss spectroscopy, photoemission spectroscopy and ellipsometry, and theoretically by first principle calculations [1, 9–17]. Experimental studies [1, 9–11, 14, 15] showed that α-SnS is a narrow-gap semiconductor with an indirect band-gap of 1.07–1.25 eV and that the direct band-gap is located at slightly higher energies of 1.296–1.39 eV. The *ab initio* calculations gave the somewhat higher values of 1.19–1.6 eV for the indirect and 1.8 eV for the direct band-gap [15, 17]. The optical properties of α-SnS were studied by optical, infrared and Raman spectroscopy and a pronounced anisotropy of the optical constants was observed [10, 18, 16]. A second-order high-temperature phase transition was reported for SnS. The α polymorph transforms at 878 K to the more symmetric β-SnS ($Cmcm$, B33) [19, 20].

The influence of high pressure and temperature on the electronic band-gap in SnS was studied by Parenteau and Carlone [13] using optical absorption spectroscopy. With increasing pressure, reductions of the direct and indirect band-gaps were observed, with the decrease of the direct gap being larger than the reduction of the indirect band-gap.

Peters and McNeil [21] studied the high-pressure behaviour of SnSe, which is isostructural to α-SnS, up to 14 GPa using ^{119}Sn Mössbauer spectroscopy. In the pressure range from ambient pressure to 3.3 GPa, pronounced changes in the isomer shift, the quadrupole splitting and the effective thickness of the sample were found. The observed changes above 3.3 GPa were significantly smaller. The authors attribute this behaviour to the rapid change of the

interlayer distances at lower pressures and the small changes of the intralayer distances in the high-pressure region.

High-pressure x-ray diffraction studies on the isostructural compounds GeS [22], GeSe [23, 24] and SnSe [25] up to 10, 80 and 34 GPa, respectively, revealed a large anisotropy of the lattice compression. Although a discontinuity in the resistivity curve of GeSe was observed at 25 GPa [24] no further evidence for a pressure-induced structural phase transition in these compounds was provided.

Surprisingly little is known about the elastic properties of SnS. Hence, the goal of the work presented here was to measure the structural changes induced by the application of hydrostatic pressure in order to elucidate the compression mechanism of α-SnS and to determine precisely the equation-of-state. Here, the results of a high-pressure synchrotron powder-diffraction study of α-SnS up to 38 GPa are reported.

2. Experimental details

SnS was crystallized from the elements by high-temperature synthesis. A stoichiometric mixture of tin and sulfur was sealed in an evacuated silica tube, kept at 1173 K for 5 days and gradually cooled to room temperature. The phase content of the reaction product was analysed using conventional x-ray powder diffraction and the stoichiometry of the sample was verified by electron microprobe analysis using a Cameca Camebax microprobe. The results confirm that the product is a single phase and of ideal composition within experimental errors.

The diffraction experiments were performed at the beamline ID30 at the ESRF in Grenoble, France. High-pressure, ambient temperature powder diffraction patterns were collected at a wavelength of $\lambda = 0.3738$ Å using a MarResearch (mar345) image-plate detector with a spatial resolution of $100 \times 100\ \mu m^2$. The incident beam was focused to $30 \times 30\ \mu m^2$ at the sample position. In order to improve the powder average, an array of 3×3 points on the specimen was sampled with the x-ray beam for 4 s at each position, giving a total exposure time of 36 s/image. Pressure up to 38 GPa was applied using a membrane driven diamond anvil cell. The sample was placed in the hole (diameter $= 200\ \mu m$) of an Inconel gasket preindented to 80 μm. In order to ensure quasi-hydrostatic conditions nitrogen was used as a pressure transmitting medium. The ruby fluorescence method was used for the pressure determination applying the Mao pressure scale [26]. A silicon standard placed at the sample position was measured to determine the sample-to-detector distance. Geometry parameters for the radial integration of the two-dimensional data were determined using FIT2D [27]. For the transformation into standard one-dimensional powder patterns the software TWO2ONE [28] was used, which allows for counting statistics of multiply measured data points in order to provide proper error estimates of the intensities and hence a correct weighting scheme in subsequent least-squares refinements [29].

Lattice parameters were obtained from whole-powder-pattern refinement and the structure of the low pressure phase was refined by the Rietveld method, employing the program FULLPROF [30]. The background was described by linear interpolation between selected points and the peak profiles were modelled using the pseudo-Voigt function [31]. The standard deviations of the refined parameters were scaled with the Bérar-factor [32]. The pressure–volume data were fitted by Birch–Murnaghan equations-of-state [33].

3. Results and discussion

X-ray powder diffraction patterns were collected from atmospheric pressure up to 38.5(1) GPa. The patterns consist only of peaks from SnS, reflections from the pressure transmitting medium

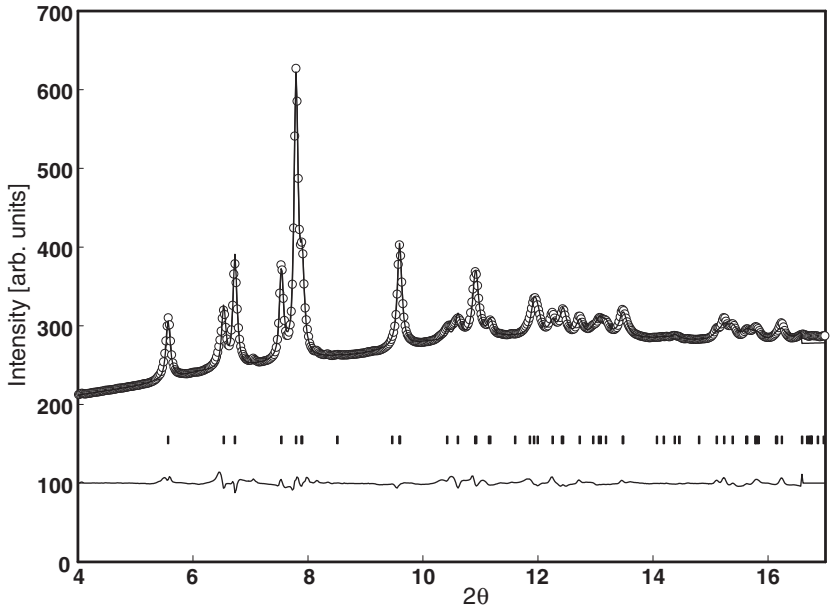

Figure 2. Observed (circles) and calculated (solid curve) diffraction pattern for α-SnS at 4.29(6) GPa (R_p: 10.2, R_{wp}: 8.93, χ^2: 1.86). The difference curve between the measured and calculated intensities and the tick marks for the calculated reflection positions are plotted at the bottom of the figure.

or gasket material were not observed. As a representative example of the obtained data quality, the observed and calculated diffraction patterns resulting from the Rietveld refinement of the data at 4.29(6) GPa are presented in figure 2.

Between 15.9 and 18.1 GPa a phase transition was found from sudden changes in the intensity distribution and peak positions.

The diffraction pattern at 18.1(1) GPa was used for indexing, employing the program *Dicvol91* [34]. All diffraction patterns above 18.1(1) GPa could be indexed with a monoclinic unit cell in the space group $P2_1/c$. The lattice parameters of the high-pressure phase were determined by whole-powder-pattern refinement. The values of the lattice parameters at 18.1(1) GPa were refined to $\mathbf{a} = 11.294(2)$ Å, $\mathbf{b} = 3.654(1)$ Å, $\mathbf{c} = 7.217(1)$ Å and $\beta = 112.41(2)^\circ$. The unit cell transformation relation between the orthorhombic α-SnS and the monoclinic γ-SnS is expressed by the following transformation matrix:

$$(\mathbf{a_o}, \mathbf{b_o}, \mathbf{c_o}) \begin{pmatrix} 1 & 0 & 0 \\ 0 & 1 & 0 \\ \bar{1} & 0 & 2 \end{pmatrix} = \begin{pmatrix} \mathbf{a_m} \\ \mathbf{b_m} \\ \mathbf{c_m} \end{pmatrix}.$$

The observed and calculated diffraction pattern at 36.1(1) GPa of the high-pressure data from γ-SnS resulting from the whole-powder-pattern refinement is shown as an example in figure 3. Figure 4 shows the pressure dependence of the unit cell volumes for α and γ-SnS. The pressure dependence of the lattice parameters is shown in figure 5.

The linear compressibilities of the α-SnS phase were derived from fits of Birch–Murnaghan equations-of-state to the cubed lattice parameters in the low pressure region. They are $k_\parallel \mathbf{a} = 0.0122(6)$ GPa^{-1}, $k_\parallel \mathbf{b} = 0.0036(2)$ GPa^{-1} and $k_\parallel \mathbf{c} = 0.0080(3)$ GPa^{-1}. The unit cell volume at zero pressure V_0, the bulk modulus B_0 and the pressure derivative of the bulk modulus $B' = \partial B_0/\partial p$ were determined by fitting of Birch–Murnaghan equations-of-state

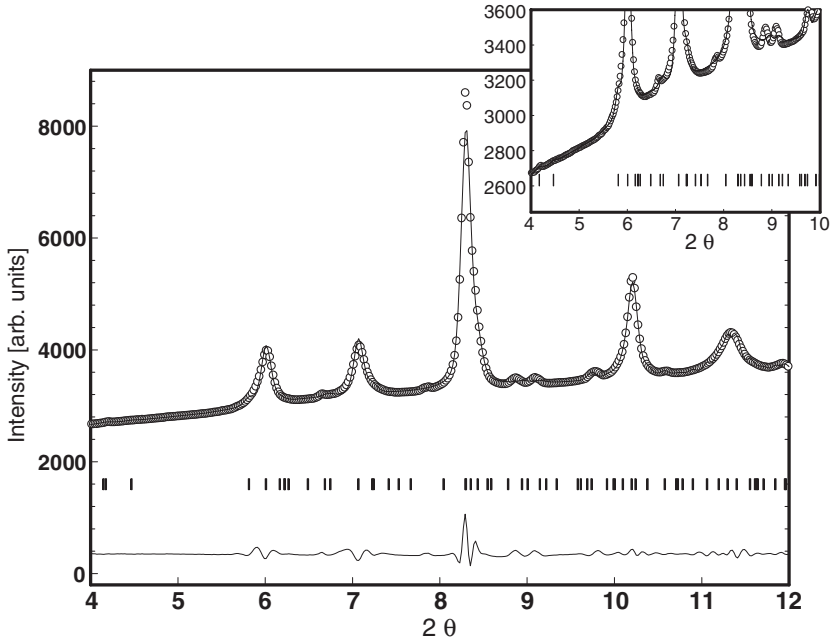

Figure 3. Observed (circles) and calculated (solid curve) diffraction pattern for γ-SnS at 36.1(1) GPa (R_p: 13.6, R_{wp}: 13.5, χ^2: 1.78). The difference and the tick marks for the calculated reflection positions are plotted at the bottom of the figure. The inset shows a magnification of the diffraction pattern for a better visualization of the weak super-structure reflections.

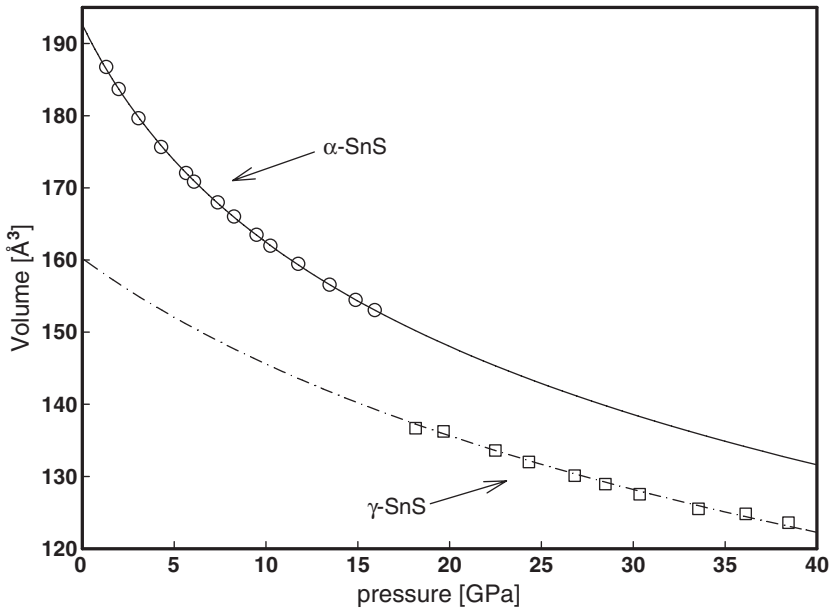

Figure 4. Pressure dependence of the unit cell volume of α-SnS (○) and γ-SnS (□). The curves result from the fits of a third-order Birch–Murnaghan equation-of-state (solid) to the low pressure and a second Birch–Murnaghan equation-of-state (dashed curve) to the high pressure phase. The experimental error bars are equivalent to the size of the symbols.

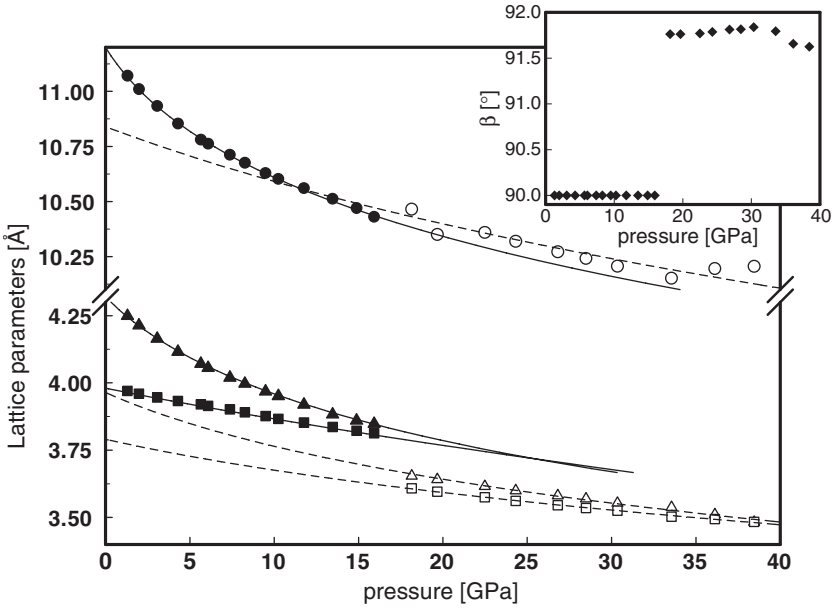

Figure 5. Pressure dependence of the unit cell parameters **a** (○), **b** (□) and **c** (△). The monoclinic lattice parameters were transformed into the orthorhombic setting (**a** sin β, **b**, **c**/2). The filled symbols represent the low pressure α-SnS and the open symbols the high-pressure γ phase. The evolution of the angle β with pressure is shown in the inset.

Table 1. Values of the equations-of-state for several isostructural metal monochalcogenides. The volumes at zero pressure V_0 are normalized to 4 fu/unit cell.

	V_0 (Å^3)	B_0 (GPa)	B'	References
α-SnS	192.6(3)	36.6(9)	5.5(2)	This work
γ-SnS	160(1)	86.0(5)	4	This work
GeSe		40.7(3.5)	5.0(4)	[24]
		47.5	5.1	[25]
		43.1(5)	4	[23]

to the volume data. The results of the fits are given in table 1. The bond lengths in the tin coordination polyhedra resulting from the Rietveld refinement of the α-SnS structure up to the transition pressure are presented in table 2.

The value of $V_0 = 192.6(3)$ Å^3 obtained from the fit of a third-order Birch–Murnaghan equation-of-state to the volume data of α-SnS agrees well with the data given by [7]. The values obtained for the bulk modulus $B_0 = 36.6(9)$ GPa and the pressure derivative of the bulk modulus $B' = 5.5(2)$ also compare well with the values for the isostructural compounds given in table 1. The fit of a second-order Birch–Murnaghan equation-of-state to the volume data of the high-pressure polymorph γ-SnS resulted in a volume at zero pressure V_0 of 160(1) Å and a bulk modulus B_0 of 86.0(5) GPa. The high-pressure phase, γ-SnS, is about two times less compressible than the α-SnS polytype. The lattice compression of α-SnS is highly anisotropic. The linear compressibility parallel to the stacking direction of the layers **a** is 1.5 times higher than along the **c** direction and 3.4 times higher than parallel to the **b** direction. These values are in good agreement with the previously reported results for GeS and GeSe [23, 22].

Table 2. Pressure dependence of the Sn–S bond distances in α-SnS with values given in ångströms. The sulfur atoms occupy the following positions or symmetry equivalent positions S(1) $x - 0.5$, 0.25, $0.5 - z$, S(3, 5) $-x$, 0.75, $-z$, S(4) $x - 1$, 0.25, $z - 1$, S(6, 8)$1 - x$, 0.75, $-z$ and S(7) $x - 1$, 0.25, z.

p (GPa)	S(1)	S(3, 5)	S(6, 8)	S(4)	S(7)
1.30(5)	2.51(2)	2.68(3)	3.22(2)	3.42(1)	4.08(3)
1.98(5)	2.50(3)	2.68(2)	3.17(1)	3.39(2)	4.05(2)
3.06(4)	2.51(2)	2.67(1)	3.13(2)	3.35(1)	3.97(3)
4.29(6)	2.49(1)	2.67(2)	3.08(2)	3.33(3)	3.92(4)
5.65(4)	2.46(2)	2.67(2)	3.04(1)	3.34(2)	3.85(3)
6.08(5)	2.46(3)	2.71(3)	2.99(2)	3.31(1)	3.86(3)
7.37(4)	2.54(2)	2.68(2)	2.96(1)	3.23(3)	3.75(4)
8.26(5)	2.61(3)	2.71(1)	2.88(2)	3.13(2)	3.67(2)
9.48(3)	2.62(2)	2.71(3)	2.85(1)	3.11(1)	3.61(2)
10.24(5)	2.62(2)	2.71(2)	2.83(2)	3.11(2)	3.59(3)
11.76(7)	2.66(1)	2.72(2)	2.78(2)	3.08(3)	3.50(3)
13.46(6)	2.64(3)	2.72(1)	2.74(1)	3.10(2)	3.43(2)
14.88(8)	2.61(2)	2.64(3)	2.80(4)	3.12(3)	3.42(3)
15.92(2)	2.57(3)	2.61(3)	2.82(5)	3.26(5)	3.29(5)

The pronounced anisotropy of the compression of α-SnS can be understood by considering the different types of bonding in the structure. The Sn–S bond lengths in the tin coordination-polyhedron range from 2.51(2) to 3.42(1) Å (table 2). The individual Sn–S bonds show different compression behaviour. While the bonds in the **bc**-plane of the layer decrease by 1.5% and 13.0% for Sn–S(3) and Sn–S(6), the Sn–S(1) bond increases by 3.9%, thus inducing an effective expansion of the layer along their stacking direction. This can be attributed to increasing repulsive forces between the sulfur atoms in the layers due to decreasing S–S distances with pressure. Such a behaviour has been observed in a series of layered chalcogenide compounds, e.g. 2H-MoS_2, TiS_2, SnS_2, 3R-NbS_2 [35–38]. The inter-layer Sn–S bonds are more compressible than the intra-layer bonds. The Sn–S(4) and the Sn–S(7) bonds are shortened by 8.8% and 19.4%, respectively. With increasing pressure the S(7) atom is driven into the first coordination sphere of the tin atom, changing its local environment from six- to sevenfold coordination.

The phase transition is accompanied by a pronounced volume discontinuity of 9.1% at 15.92(2) GPa. This is mainly caused by a drop in the **b** and **c** lattice parameters, whereas the compression along the **a** direction remains essentially unaffected. Unfortunately, the quality of the data beyond the phase transition was not sufficient for a structure determination of the high-pressure γ-SnS phase. Taking into account the individual compression behaviour of the lattice parameters, a distinct change in the layers (e.g. corrugation or relaxation of the layer) or a layer shift with a translation vector in the (011)-plane can be proposed as the transition mechanism. The continuous compression behaviour along the stacking direction **a** shows that the compression of the van-der-Waals gap is not yet depleted and might still be considered as a dominant compression mechanism in the high-pressure phase.

The phase transition can be described by analysing the symmetry relationships between the two space groups $Pnma$ and $P2_1/c$ in terms of *klassengleiche* (index k) and *translationengleiche* (index t) subgroups. For the given unit cells of the two phases the indirect group/subgroup relationship

$$Pnma \xrightarrow{t2} P2_1/m \xrightarrow{k2\ \mathbf{a}-\mathbf{c},\mathbf{b},\mathbf{2c}} P2_1/c$$

exists. The large volume discontinuity together with the indirect group/subgroup relationship points to a first-order reconstructive character of the transition. Furthermore, the phase

transformation is improper ferro-elastic having a critical wavevector associated with the change in the translation symmetry of $(1/2, 0, 1/2)$ located at the U-point of the Brillouin zone [39].

Unfortunately, the crystal structure of the high-pressure phase could not be solved on the basis of the presently available experimental data. A strong peak overlap in the high-pressure phase had to be taken into account (figure 3), which is induced by the small metric differences of the cell parameters as well as by a strain-broadening of the reflection profile that certainly cannot be excluded from being present at pressures above 15 GPa with nitrogen as the pressure transmitting medium. The strong peak overlap made an *ab initio* structure determination from the powder data impossible since a sufficient number of independent structure factors could not be extracted from the profile fit. Refinements of structural models obtained by (i) the transformation of the atomic coordinates according to the symmetry relationship given above, and (ii) direct and energy minimization approaches failure. They either did not converge or did not yield meaningful results being in accordance with the known crystal chemistry of high-pressure phases of general formula AB.

Very recently, a phenomenological theory of the reconstructive phase transition between the NaCl (B1) and CsCl (B2) structure types in binary compounds was reported [40]. The authors proposed a general transition mechanism consisting of two consecutive anti-parallel displacements along the cubic [110] direction of atomic bilayers stacked along the respective [001] direction. This mechanism gives rise to intermediate structures of the B16 and B33 type. The proposed B1–B16–B33–B2 sequence of transitions is partially or fully observed in the group IV monochalcogenides. The intermediate structures are very similar to α-SnS. However, in this comprehensive review a monoclinic distortion is only reported to occur to space group $P2_1$ in the case of AgCl [41]. Furthermore, the direction of the layer shift is different to that in all other examples. In order to understand how SnS fits into the scheme of high-pressure phases of AB compounds, further experiments, with improved data quality are needed. This includes the use of a strictly hydrostatic pressure-transmitting medium such as He or Ne and possibly a thermal relaxation by means of *in situ* resistive or laser heating.

4. Summary and conclusions

The high-pressure behaviour of α-and γ-SnS was studied up to 38.4(1) GPa. Bulk moduli and their pressure derivatives were determined for both polytypes. The structural phase transformation observed at 18.1 GPa from the orthorhombic α-SnS to the monoclinic γ-phase was characterized as a reconstructive first-order improper ferro-elastic transition. A possible mechanism for the phase transition was proposed on the basis of the lattice compression. Since the determination of atomic positions for the high-pressure γ-phase was not possible, further investigations are required.

Acknowledgments

LE, KK and AK would like to thank the European Union for support under the TMR program. LE is grateful to the German Science Foundation (DFG) for funding under grants De 412/21-1 and FOR 345/1-1 and support through the Carnegie Institution of Washington.

References

[1] Shalvoy R B, Fisher G B and Stiles P J 1977 X-ray photoemission studies of the valence bands of nine IV–VI compounds *Phys. Rev.* B **15** 2021–4

[2] Trbojevic D, Nikolic P M, Perovic B and Cekic V 1981 Photovoltaic detectors in SnS produced by Sb^+ ion implantation *Appl. Phys. Lett.* **38** 362–4
[3] Subramanian B, Sanjeeviraja C and Jayachandran M 2001 Cathodic electrodeposition and analysis of SnS films for photoelectrochemical cells *Mater. Chem. Phys.* **71** 40–6
[4] Nabi Z, Kellou A, Méçabih S, Khalfi A and Benosman N 2003 Opto-electronic properties of rutile SnO_2 and orthorhombic SnS and SnSe compounds *Mater. Sci. Eng.* B **98** 104–15
[5] Hofmann W 1935 Die Struktur von Zinnsulfür und Teallit *Fortschr. Mineral.* **19** 30
[6] Hofmann W 1935 Ergebnisse der Strukturbestimmung komplexer Sulfide *Z. Kristallogr.* **92** 161–73
[7] Wiedemeier H and von Schnering H G 1978 Refinement of the structures of GeS, GeSe, SnS and SnSe *Z. Kristallogr.* **148** 295–303
[8] Ramdohr P 1935 Vorkommen und Eigenschaften des Herzenbergits *Z. Kristallogr.* **92** 186–9
[9] Anderson J S and Morton M C 1945 The electrical conductivity of stannous sulphide *Proc. R. Soc.* A **184** 83–101
[10] Lambros A P, Geraleas D and Economou N A 1974 Optical absorption edges in SnS *J. Phys. Chem. Solids* **35** 537–41
[11] Otto A, Ley L, Azoulay J, Grandke T, Eymard R, Braun W and Cardona M 1977 Electron–hole interaction in the d-electron excitations of GeS and SnS *Phys. Rev.* B **16** 4429–33
[12] Eymard R and Otto A 1977 Optical and electron-energy-loss spectroscopy of GeS, GeSe, SnS, and SnSe single crystals *Phys. Rev.* B **16** 1616–23
[13] Parenteau M and Carlone C 1990 Influence of temperature and pressure on the electronic transitions in SnS and SnSe semiconductors *Phys. Rev.* B **41** 5227–34
[14] Taniguchi M, Johnson R L, Ghijsen J and Cardona M 1990 Core excitons and conduction-band structures in orthorhombic GeS, GeSe, SnS, and SnSe single crystals *Phys. Rev.* B **42** 3635–42
[15] Ettema A R H F, de Groot R A, Haas C and Turner T S 1992 Electronic structure of SnS deduced from photoelectron spectra and band-structure calculations *Phys. Rev.* B **46** 7363–73
[16] Yu L-M, Degiovanni A, Thiry P A, Ghijsen J and Caudano R 1993 Infrared optical constants of orthorhombic IV–VI lamellar semiconductors refined by a combined study using optical and electronic spectroscopies *Phys. Rev.* B **47** 16222–8
[17] Kellö V, Sadlej A J and Fægri K Jr 1998 Electronic correlation and relativistic contributions to dipole moments of heavy oxides and sulfides: SnO, PbO, SnS, and PbS *J. Chem. Phys.* **108** 2056–66
[18] Chandrasekhar H R, Humphreys R G, Zwick U and Cardona M 1977 Infrared and Raman spectra of the IV–VI compounds SnS and SnSe *Phys. Rev.* B **14** 2177–83
[19] Wiedemeier H and Csillag F J 1979 The thermal expansion and high temperature transformation of SnS and SnSe *Z. Kristallogr.* **149** 17–29
[20] von Schnering H G and Wiedemeier H 1981 The high temperature structure of β-SnS and β-SnSe and the B16–B33 type λ-transition path *Z. Kristallogr.* **156** 143–50
[21] Peters M J and McNeil L E 1990 High-pressure Mössbauer study of SnSe *Phys. Rev.* B **41** 5893–7
[22] Hsueh H C, Warren M C, Vass H, Ackland G J, Clark S J and Crain J 1996 Vibrational properties of the layered semiconductor germanium sulfide under hydrostatic pressure: theory and experiment *Phys. Rev.* B **53** 14806–17
[23] Hsueh H C, Vass H, Clark S J, Ackland G J and Crain J 1995 High-pressure effects in the layered semiconductor germanium selenide *Phys. Rev.* B **51** 16750–61
[24] Onodera A, Akamoto I, Fujii Y, Mori N and Sugai S 1997 Structural and electrical properties of GeSe and GeTe at high pressure *Phys. Rev.* B **56** 7935–41
[25] Chattopadhyay T, Werner A and von Schnering H G 1983 Pressure induced phase transitions in IV–VI compounds *Materials Research Society Proc.* vol 22, ed C Howman, R K MacCrone and E Whally (New York: North-Holland) p 93
[26] Mao H K, Bell P M, Shaner J W and Steinberg D J 1978 Specific volume measurements of Cu, Mo, Pd, and Ag and calibration of the ruby R_1 fluorescence pressure gauge from 0.06 to 1 Mbar *J. Appl. Phys.* **49** 3276–83
[27] Hammersley A P, Svensson S O, Hanfland M, Fitch A N and Häusermann D 1996 Two-dimensional detector software: from real detector to idealised image or two-theta scan *High Pressure Res.* **14** 235–50
[28] Vogel S, Ehm L, Knorr K and Braun G 2002 Automated processing of 2D powder data *Adv. X-ray Anal.* **45** 31–3
[29] Chall M, Knorr K, Ehm L and Depmeier W 2000 Estimating intensity errors of powder diffraction data from area detectors *High Pressure Res.* **17** 315–23
[30] Rodriguez-Carvajal J 1993 Recent advances in magnetic structure determination by neutron powder diffraction *Physica* B **192** 55–69
[31] Thompson P, Cox D E and Hastings J B 1987 Rietveld refinement of Debye–Scherrer synchrotron x-ray data from Al_2O_3 *J. Appl. Crystallogr.* **20** 79–83

[32] Bérar J-F and Lelann P 1991 E.s.d.'s and estimated probable error obtained in Rietveld refinements with local correlations *J. Appl. Crystallogr.* **24** 1–5
[33] Birch F 1978 Finite strain isotherm and velocities for single-crystal and polycrystalline NaCl at high pressures and 300° *J. Geophys. Res.* **83** 1257–68
[34] Boultif A and Louër D 1991 Indexing of powder diffraction patterns from low-symmetry lattices by the successive dichotomy method *J. Appl. Crystallogr.* **24** 987–93
[35] Webb A W, Feldman J L, Skelton E F, Towle L C, Liu C Y and Spain I L 1976 High pressure investigations of MoS_2 *J. Phys. Chem. Solids* **37** 329–35
[36] Allan D R, Kersey A A, Clark S J, Angel R J and Ackland G J 1998 High-pressure semiconductor–semimetal transition in TiS_2 *Phys. Rev.* B **57** 5106–10
[37] Knorr K, Ehm L, Hytha M, Winkler B and Depmeier W 2001 The high pressure behaviour of SnS_2: x-ray powder diffraction and quantum mechanical calculations up to 10 GPa *Phys. Status Solidi* b **223** 435–40
[38] Ehm L, Knorr K and Depmeier W 2002 High-pressure behaviour of 3R-NbS_2 *Z. Kristallogr.* **217** 522–4
[39] Stokes H T and Hatch D M 1988 *Isotropy Subgroups of the 230 Crystallographic Space Groups* (Singapore: World Scientific)
[40] Toledano P, Knorr K, Ehm L and Depmeier W 2003 Phenomenological theory of the reconstructive phase transitions between NaCl and CsCl structure types *Phys. Rev.* B **67** 144106
[41] Kusaba K, Syono Y, Kikegawa T and Shimomura O 1995 A topological transition of B1–KOH–TlI–B2 type AgCl under high-pressure *J. Phys. Chem. Solids* **56** 751–7